

Astronomical Site Selection Scenarios for Asia

Abdulvahap Yılmaz 601

¹Health Services Vocational School, Erzincan Binali Yıldırım University, Erzincan, Türkiye.

Keywords: Observatory, Site selection, Infrared-Radio-Optical, MCDA

Abstract

This study aimed to identify and evaluate suitable areas for astronomical observations in Asia using Geographic Information System (GIS) and Multi-Criteria Decision Analysis (MCDA) methods. Our study provides spatial coverage with satellite-based datasets to determine the ideal astronomical areas in Asia for future telescope construction. These datasets were created by adding a digital elevation model (DEM) and artificial light (AL) along with atmospheric data such as cloud cover (CC), precipitation water vapor content (PWV), aerosol optical density (AOD), and wind speed (WS). The dataset was analyzed using a combination of MCDA and GIS techniques. On the continent, the Tibetan Plateau and its surroundings (except the area around $90^{\circ}E-35^{\circ}N$) in northern China were identified as the most suitable areas for astronomical studies with radio telescopes. Suitable areas for infrared and optical telescopes are mainly found in the southeast of the Tibetan Plateau (around $83^{\circ}E-31^{\circ}N$). According to the analysis, an area of $369,096 \ km^2$, which corresponds to approximately 0.83% of the continent, is best suited for infrared observations. Approximately 3.87% of the continent, that is, about $1,725,246 \ km^2$, is best suited for radio telescopes, while 0.8%, that is, $355,842 \ km^2$, is best suited for observations with optical telescopes. The Corona-Borealis Observatory (Ngari) is located in the most ideal location for all three scenarios. The findings of this study are of great importance for future plans for astronomical sites on the continent.

Resumen

El objetivo de este estudio es identificar y evaluar áreas adecuadas para observaciones astronómicas en Asia utilizando métodos del Sistema de Información Geográfica (SIG) y el Análisis de Decisiones Multicriterio (MCDA). Nuestro estudio proporciona cobertura espacial mediante conjuntos de datos satelitales para determinar zonas astronómicas ideales en Asia. Estos conjuntos de datos se crearon combinando un modelo digital de elevación (DEM) y la luz artificial (AL), junto con variables atmosféricas como la cobertura de nubes (CC), el contenido de vapor de agua precipitable (PWV), la densidad óptica de aerosoles (AOD) y la velocidad del viento (WS). El conjunto de datos fue analizado utilizando una combinación de técnicas MCDA y SIG. En el continente, la meseta tibetana y sus alrededores (excepto el área en torno a 90°E–35°N), en el norte de China, fueron identificados como las zonas más adecuadas para estudios astronómicos con radiotelescopios. Las áreas óptimas para telescopios infrarrojos y telescopios ópticos se localizan principalmente en el sureste de la meseta tibetana (alrededor de 83°E–31°N). Según el análisis, un área de 369,096 km², que corresponde aproximadamente al 0.83 % del continente, es ideal para observaciones infrarrojas. El 3.87 % del continente, es decir, aproximadamente 1,725,246 km², es adecuado para radiotelescopios, mientras que el 0.8 %, o sea 355,842 km², es óptimo para observaciones con telescopios ópticos. El Observatorio Corona-Borealis (Ngari) se encuentra en la ubicación más adecuada para los tres escenarios. Los hallazgos del estudio son de gran relevancia para la planificación futura de emplazamientos astronómicos en el continente.

Corresponding author: Abdulvahap Yilmaz E-mail address: abdulvahap.yilmaz@erzincan.edu.tr Received: June 4, 2025 Accepted: August 11, 2025

1. INTRODUCTION

Asia, the largest continent on Earth (Prange & Kattenbach, 2019), covers 30% of the planet's land area (approximately 44.5 million square kilometers) and is the most populous continent in the world (over 4.5 billion inhabitants). This continent encompasses a variety of climate zones (such as deserts, tropical rainforests, and tundras) and vast and extreme geographical diversity of the world. The Rub'al-Khali Desert on the Arabian Peninsula is one of the hottest and driest regions in the world (Sultan et al., 2008), whereas Cherrapunji in Northeast India receives some of the highest rainfall in the world (average 11.7 mm/year) (Nag, 2015). Asia has the highest land mass above sea level compared with other continents. The continent's highest peak is Mount Everest

(8.848 m), which is also the highest point in the world (Firth et al., 2008). Asia is the second highest continent in the world, with an average altitude of about 950 meters, following Antarctica at 2,200 m.¹ The Verkhoyansk and Oymyakon regions in Siberia have the lowest temperatures on Earth (approximately -67.7 °C) (Box & Choi, 2003). These peculiarities of Asia are of great importance in astronomy and scientific research. Areas with high altitudes and dry climates offer ideal conditions for astronomical observations. For example, the The Five-hundred-meter Aperture Spherical Telescope (FAST), an important astronomical observation project in Asia, is located in the Dawodang depression, a natural basin

¹https://banogyani.com/7-continents-of-world-upsc-hpas-geography-notes/

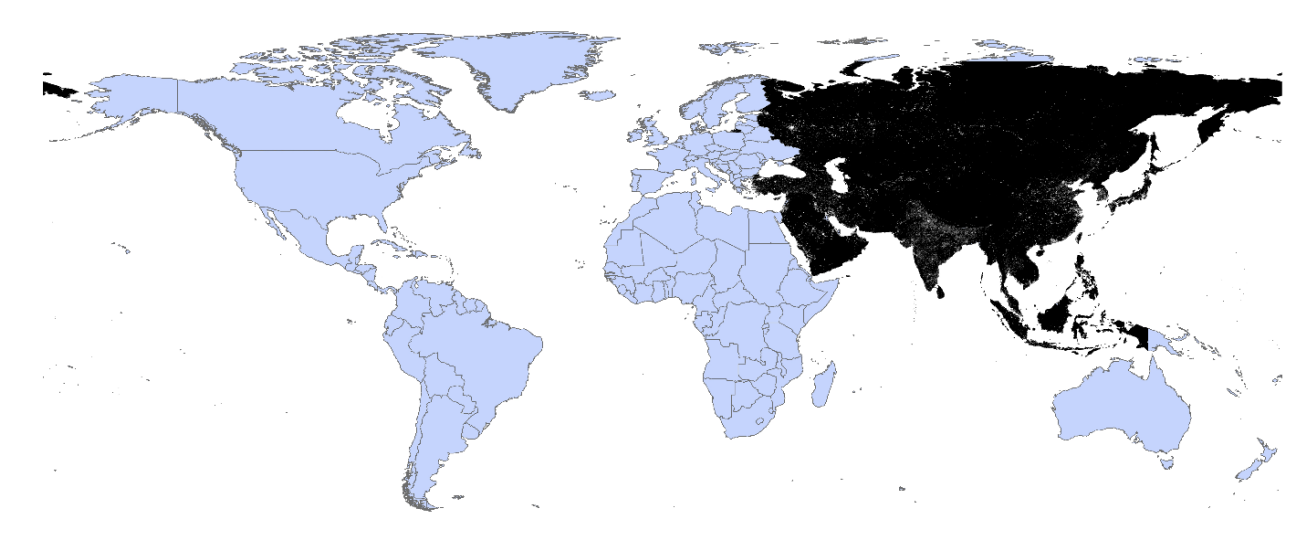


Figure 1. The Asian continent is shown on the political map of the world (without the Antarctic continent) as a clearly black background. The image of the Asian continent distributed with white dots on this black background represents the artificial light (AL) data obtained from the VIIRS-DNB data (day/night band) (values above 75° 20′ 18″ latitude are not included in the AL dataset). The white dots on the black background are the view from space of the brightness produced during the night, especially in densely populated and industrialized regions.

Table 1. Coordinates of some astronomical stations in Asia and parameter values of the stations used in the study.³

A	T 1	Latitude	AL	WS	PWV	DEM	CC	4.O.D.
Astronomical Units	Longitude		(nW/cm ² /sr)	$(m s^{-1})$	(mm)	(m)	(%)	AOD
Corona Borealis Observatory Ngari	80.026	32.326	0.43	4.98	1.90	4965	0.20	0.25
Himalayan Chandra Telescope IAO Hanle	78.96	32.78	0.45	4.70	46.13	4278	0.20	0.07
Lijiang Station Yunnan Observatories	100.03	26.71	0.45	4.14	14.28	3193	0.51	0.12
Eastern Anatolia Observatory DAG	41.23	39.78	0.62	7.32	5.48	2989	0.37	0.17
Terskol	42.5	43.27	2.72	1.41	10.79	2820	0.62	0.22
ISON-Terskol Observatory	42.5	43.740	0.66	10.70	10.12	2810	0.49	0.22
Tokyo-Norikura	137.56	36.11	0.74	2.89	15.63	2791	0.68	0.12
Assah	77.87	43.23	0.54	3.34	5.72	2662	0.42	0.12
Lulin Observatory	120.87	23.47	0.35	1.13	32.62	2634	0.32	0.84
Tien-Shan Astronomical Observatory	76.97	43.06	51.51	0.76	11.89	2581	0.54	0.20

in Pingtang County, Guizhou, southwestern China, and is the largest single-dish radio telescope in the world (Nan, 2006).

In this study, Asia is considered according to the geographical continent definition (see Figure 1)². Countries in the Middle East (partially), South Asia, Central Asia, and Southeast Asia were included in this analysis based on geographical boundaries rather than cultural identities. The astronomical stations in Asia are listed in Table 1. Meteorological, geographical, and anthropogenic data from these stations provide information on the suitability of the station locations for astronomical studies.

Quantitative and spatial analyses were used to determine the most ideal locations on the continent for astronomical observation. In this study, a GIS layer was created for each quantitative parameter using meteorological, geographic, and anthropogenic datasets. The use of remote access methods for the creation of quantitative datasets and geographic information systems (GIS) in the analysis process offers advantages in terms of time, cost, and efficiency. In a global study conducted by Aksaker et al. (2020) using remote access methods and GIS, suitable areas for astronomical studies were identified on a country-by-country basis, and as a result of the study, the Andes and the China/Tibet Plateau were suggested as the most ideal locations for astronomical studies. In another study (Aksaker et al., 2024), the most ideal locations for astronomical studies on the Antarctic continent were proposed for infrared, optical, and submillimeter telescopes. Depending on the wavelength sensitivity of the instruments used in astronomical studies, suitable astronomical areas may vary. Therefore, different astronomical layers and weights can be used to create different scenarios. This study aims to provide useful information for professionals, amateurs, and official institutions in the field of astronomy and to propose the most suitable astronomical areas for the entire Asian continent (for infrared, optical, and radio telescopes) using various parameters.

While previous studies have identified astronomical sites in individual countries on the continent, this study is the first to focus on the continent as a whole. This is the first study to use astronomical parameters and parameter weights,

²https://www.britannica.com/place/Asia

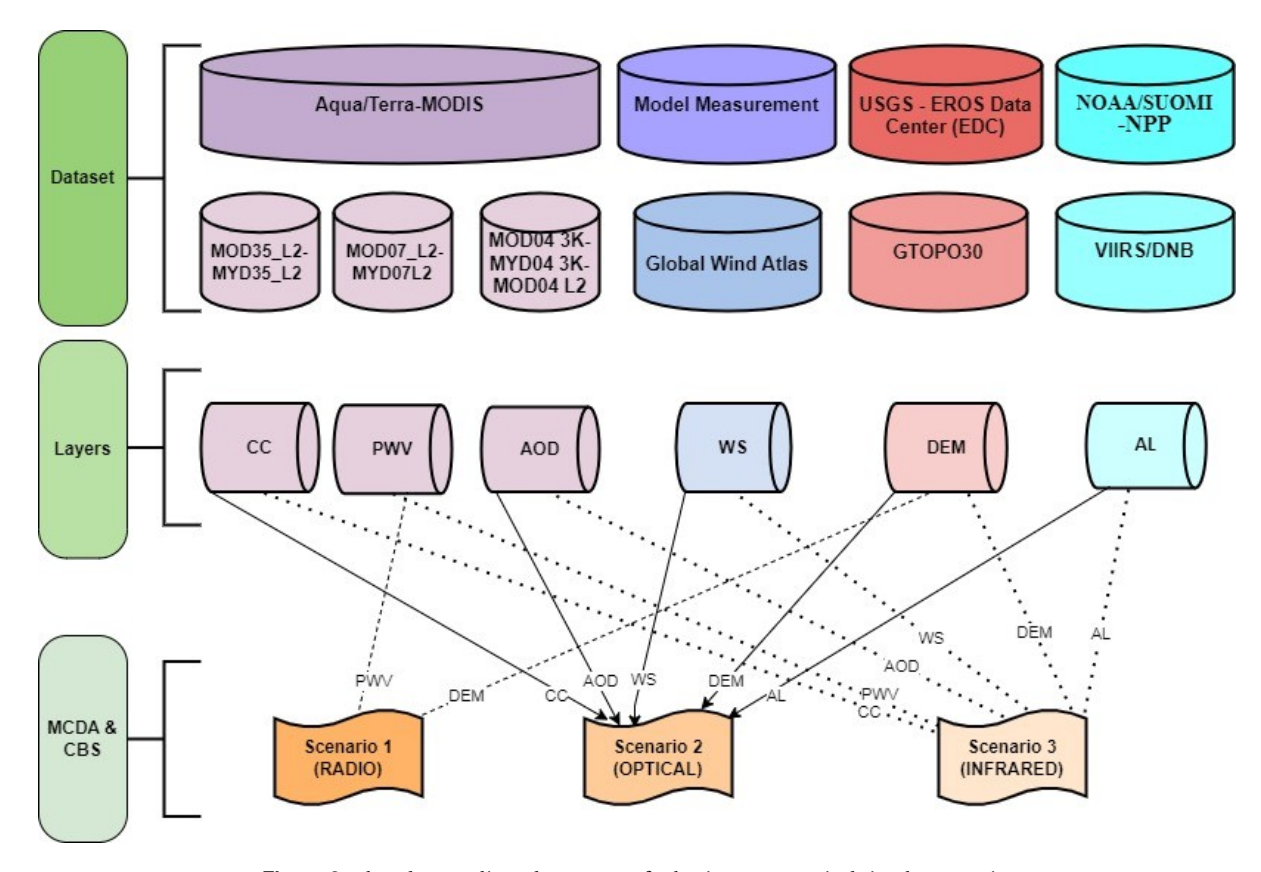


Figure 2. Flowchart outlines the process of selecting astronomical sites by scenario.

spatial boundaries (the entire Asian continent), and geographic information system (GIS) analyses. It is important to note that the areas proposed in this study should be verified through field measurements. Owing to the established demarcations, the results of this study will reduce the time and expenses for investments in astronomical sites.

2. METHODOLOGY

The flowchart shows the classification of astronomical fields into three main phases (Figure 2). The details are provided in S 2.

2.1. Data analysis

All processes in this study are shown in the flowchart (see Figure 2). The datasets were collected from various sources using remote-sensing methods. Multi-criteria decision analysis (MCDA) and geographic information systems (GIS) infrastructures were used to analyze the datasets, and different scenarios were created for selecting astronomical areas. All layers in the GIS (except the locations of the astronomical stations) were converted to GeoTIFF format and used for analysis. Each layer was classified based on its impact on the astronomical conditions, ranging from 1 for the most adverse and 5 for the most favorable conditions; all layers were weighted and overlaid (for details, see Yılmaz, 2023a,b). The layers were used at a resolution of 1 km in the WGS 1984 projection. This study focused on the landmass of the continent (water formations at continental boundaries were excluded).

2.1.1. Data sets

In this study, datasets for cloud cover (CC), precipitable water vapor (PWV), aerosol optical depth (AOD), wind speed (WS) (Badger et al., 2015), artificial light (AL) (Badger et al., 2015),

and digital elevation model (DEM) (Gesch et al., 1999) were used as atmospheric layers for site selection. The properties of the data layers are listed in Table 2. Most datasets were obtained from the Astro-GIS database (Aksaker et al., 2024). The database can be accessed at Astro GIS (https://www.astrogis.org/). The Astro GIS database (except for Antarctica in the AL dataset) provides global data in the GEOTIFF format (i.e., with a tif extension).

2.1.2. Cloud cover (CC)

Cloud cover is a measure of the extent to which the density of clouds in the atmosphere of a region affects sky visibility (Glickman, 2000). Cloud cover is a critical parameter in astronomy that significantly affects the quality and efficiency of ground-based astronomical observations. Cloud-free days with high visibility extended the observation period. Therefore, cloud cover is one of the most important parameters when selecting sites for astronomical studies (Aksaker et al., 2015); (Erasmus & Peterson, 1997); (Liu et al., 2012); (Sarazin et al., 2006). In studies on the selection of sites for astronomical observatories where similar layers are used, cloud cover has been used as the most important parameter according to the criteria weights determined by expert opinions using MCDA methods (Yılmaz, 2023a,b). In addition, Ye (2011) emphasized that cloud cover is a dominant parameter for ground-based astronomical observations and accurate meteorological forecasts (Ye, 2011). Long-term cloud cover data are important for determining the atmospheric conditions at sites where astronomical studies have been performed. He emphasized that such data are essential for maintaining optimal observation periods, especially in equatorial regions, where cloud cover can be dense (Azhar et al., 2022). Therefore, cloud cover was selected as the layer for this study.

Table 2. Properties of the GIS layers used in this study (astrogis.org)

Layer	Satellite/Instrument	Product	Resolution
Cloud Coverage (CC)	Aqua/Terra-MODIS (NASA/LAADS DAAC)	MOD35 L2 MYD35 L2	1 km
Digital Elevation Model (DEM)	USGS - EROS Data Center (EDC)	GTOP030	1 km
Precipitable Water Vapor (PWV)	Aqua/Terra-MODIS (NASA/LAADS DAAC)	MOD07 L2 MYD07 L2	5 km
Aerosol Optical Depth (AOD)	Aqua/Terra-MODIS (NASA/LAADS DAAC)	MOD04 3K MYD04 3K MOD04 L2	3 / 10 km
Artificial Light (AL)	NOAA/SUOMI-NPP	VIIRS/DNB	750 m
Wind Speed (WS)	Model Measurement	Global Wind Atlas	225 m

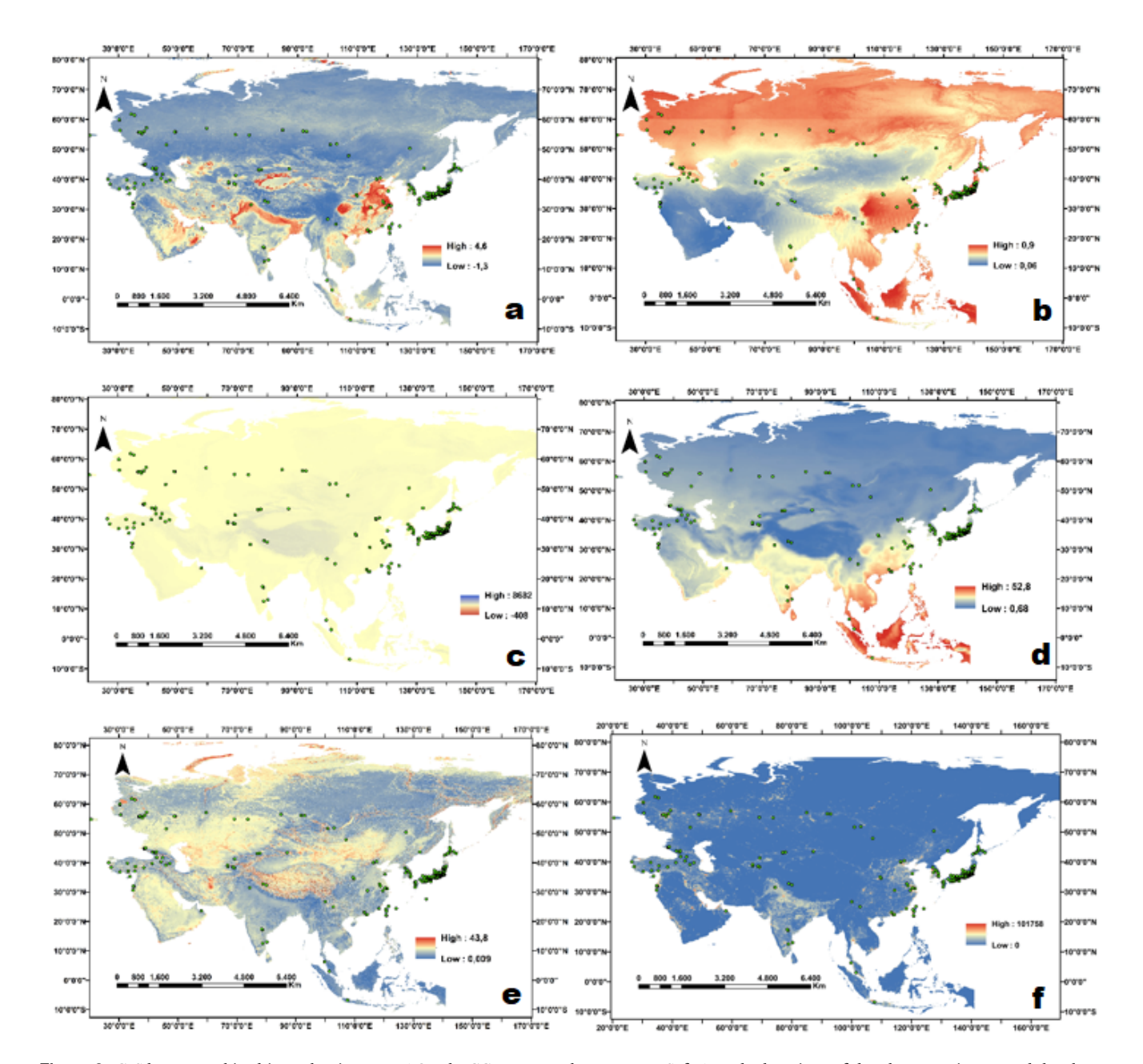


Figure 3. GIS layers used in this study Figure; a: AOD, b: CC, c: DEM, d: PWV, e: WS, f: AL. The locations of the observatories on each level are marked with green dots.

The MODIS cloud mask algorithm has proven to be a reliable solution for detecting clouds on the Terra and Aqua satellites. It classifies pixels as cloudy or clear based on spectral bands and

thresholds and has been shown to agree 85% with ground-based LiDAR measurements (Ackerman et al., 2008). However, Várnai & Marshak (2012) explained that under atmospheric conditions with

high particle density, the algorithm can misidentify some cases, which is a limitation compared to more conservative algorithms, such as CALIOP (Várnai & Marshak, 2012). Holz et al. (2008) reported that the MODIS cloud mask achieved high accuracy, especially in daylight, and in some months the accuracy was as high as 92% under clear skies. This shows that the algorithm is effective under well-lit conditions but is susceptible to seasonal bias.

Owing to the multiband approach, a more accurate distinction can be made between cloudy and clear pixels, enhancing the overall reliability (Platnick et al., 2003). MODIS satellite data are available in the HDF4 format as two different cloud cover products (MOD35 - L2 and MYD35 - L2). This data format was converted to GeoTIFF format using the Model Builder and Python codes. After conversion, both datasets were transferred to the WGS1984 projection system using the Project Raster tool. The two datasets were then merged using the Mosaic to New Raster tool and updated by integrating them into the AstroGIS database. Finally, the data obtained from the Aqua and Terra satellites were merged, and the long-term daily average of the CC dataset was calculated (Aksaker et al., 2020). The calculated values were classified as 1 (very cloudy) and 5 (cloud-free) using the Reclassify function. A map of the CC data layer is shown in Figure 3b. In Asia, the highest cloud cover is observed over large areas of northern Siberia and Russia, as well as on the islands of Southeast Asia (Indonesia and the Philippines). The lowest cloud cover was observed in southern India and the Arabian Peninsula, indicating low cloud cover in the desert and arid regions. This study provides important information on cloud cover for selecting astronomical sites in Asia.

2.1.3. Digital elevation model (DEM)

The average altitude of the Asian continent is approximately 780 m, making it the continent with the second highest average altitude after Antarctica. There are many mountains on the Asian continent that are more than eight thousand meters high. The highest peak in the world, Mount Everest, is 8,848.86 m (Firth et al., 2008). This is followed by K2 (Godwin Austen) (Walker, 1894) with a height of 8,611 m, and many other mountains can be added to this list. These mountains form the magnificent peaks of the Himalayan and Karakoram Ranges. High-altitude regions cause the formation of orographic clouds and inversion layers that increase aerosol accumulation (Houze Jr, 2012). In addition, topography controls the movement of clouds and aerosols by influencing wind flow and moisture distribution (Chen et al., 2021). Therefore, DEM is an important atmospheric parameter in astronomical site selection studies. The digital elevation model (DEM) is a map that digitally represents the elevation of the land surface and is presented in GeoTIFF format with a 1 km resolution raster dataset in GTOPO30 (Gesch et al., 1999). The dataset was classified on a scale of 1 (lowest) to 5 (highest). The map obtained from this dataset is shown in Figure 3c. The DEM data provided results similar to those of the CC. The highest regions of the Asian continent are located in the southern and central parts, especially around the Himalayas and the Tibetan Plateau. The lowest elevations are located in the western part of the continent, around the Caspian Sea and its surroundings.

2.1.4. Precipitable water vapor (PWV)

Precipitable water vapor (PWV) is an important parameter for astronomical observations, as it indicates the total water vapor present in the atmosphere, which impacts atmospheric opacity in the infrared and submillimeter range wavelengths. In particular, in the near- and mid-infrared ranges, the integrated absolute humidity represented by PWV is crucial for optimizing the observation quality (Seidel et al., 2023). The PWV varies depending on the geographical location and meteorological conditions; therefore, it is considered when determining the observation areas (Tremblin et al., 2012); (Bustos et al., 2014). Low PWV values near the observatories provide ideal conditions for improving the observation quality (Liu et al., 2012). The Moderate Resolution Imaging Spectroradiometer (MODIS) is an important data source for precipitable water vapor (PWV) owing to its advanced remote sensing capabilities. MODIS uses multiple spectral bands to generate data on water vapor at different resolutions (day and night, $1 \times 1 \text{ km}^2$ and $5 \times 5 \text{ km}^2$) and wavelengths, and is deployed on both the Terra and Aqua satellites. MODIS detects vehicle traffic primarily through near-infrared (NIR) channels (specifically around 0.865, 0.905, 0.935, 0.940, and 1.240 μ m). These channels are sensitive to the absorption properties of water vapor in the atmosphere and effectively measure water vapor. The detection process involves calculating the transmittance based on theoretical models and lookup tables derived from the HITRAN spectroscopic database (Li et al., 2003). The NIR product (MOD05) typically provides a spatial resolution of 1 km, whereas the infrared (IR) product (MOD07) provides data with a resolution of 5 km (Gurbuz & Jin, 2017). Because night sky conditions are important for astronomical site selection, infrared algorithms are preferred (Aksaker et al., 2015). The dataset was also downloaded in the HDF4 format, and the level detection process was the same as that for CC. The dataset was ranked from 1 (highest) to 5 (lowest). The layer map created from the PWV data is presented in Fig. 3d. The PWV values are high in regions with sea level and tropical climate conditions, such as Southeast Asia, the Indian subcontinent, and Indonesia. In high-altitude regions (low air temperatures), such as Central Asia, Siberia, and the Tibetan Plateau, the PWV values decreased. PWV values can be inversely related to DEM (Radionov et al., 2002).

2.1.5. Artifcial light (AL)

VIIRS DNB detects upper atmospheric radiation in the visible to near-infrared range (0.5–0.9 μm) during the night as part of the Defense Meteorological Satellite Program (DMSP) at a wavelength of about 0.7 μm and a spatial resolution of 750 m (Schueler et al., 2002). VIIRS DNB radiation measurements have high calibration accuracy, and the calibration uncertainties reported for Suomi NPP VIIRS DNB are between 2% and 6% (Chen et al., 2021). The NPP VIIRS DNB data were generated by periodic scans worldwide between approximately 01:30 and 13:30. NPP VIIRS DNB provides higher radiometric accuracy with its onboard calibration and has a dynamic range of seven orders of magnitude from approximately $3.10^{-9} \ nWcm^{-2}sr^{-1}$ to 0.02 $nWcm^{-2}sr^{-1}$, which enables the detection of extremely low light (Liao et al., 2013). The AL dataset provides important information on nighttime light levels required to analyze potential areas for constructing optical observatories. This enables the detailed mapping of artificial light sources (Falchi et al., 2016). This capability is crucial for determining optimal areas with minimal light pollution, which are ideal for astronomical studies. The AL layer created using the VIIRS cloud mask dataset for 2023 (version with outlier removal and nighttime light coverage) with the extension 'vcm-orm-ntl' in GEOTIFF format, filtered by nonartificial light sources, from (Falchi et al., 2016), is shown in Figure 3f. The layers were categorized from 1 (brightest) to 5 (faintest). The average AL values of the countries in Asia are

presented in Table 4 by converting them to the unit MPSAS (magnitude per square arcsecond) using the VIIRS DNB datasets.

$$MPSAS = 20.0 - 1.9 \log(VIIRS/DNB(AL))$$
 (1)

The eastern coastal regions of Japan, South Korea, Taiwan, and China appear to be strongly illuminated. Light pollution is highest in these regions owing to the high population density and industrial activities. In large geographical areas such as Siberia in Russia, Mongolia, and Kazakhstan, light pollution is lower owing to lower population density and less industrial activity.

2.1.6. Wind speed (WS)

Wind speed has both positive and negative effects on the site selection of astronomical observatories. The speed of air flowing over water bodies affects evaporation rates. Increased wind speed generally leads to reduced evaporation and lower humidity, whereas lower wind speeds may result in higher evaporation and increased moisture (Ravi & D'Odorico, 2005). Therefore, wind speed plays an indirect role in the selection of observatory sites, where higher wind speeds are often considered beneficial. However, high wind speeds increase the mobility of atmospheric particles and decrease atmospheric stability (Aksaker et al., 2020), making low average annual wind speeds more desirable for observational quality. It should also be noted that wind directly affects astronomical observations through atmospheric turbulence (Liu et al., 2010), and speeds above 11 m s⁻¹ may cause vibrations in telescope structures (Liu et al., 2020).

However, an important point is that the atmospheric effects of wind speed are associated with different dynamics depending on the altitude. Evaporation processes, for example, are primarily related to wind speeds near the ground, whereas optical turbulence is largely associated with high-altitude winds, such as jet streams in the upper atmosphere, particularly near the upper troposphere. The wind speed data used in this study, sourced from the Global Wind Atlas project supported by the World Bank, provide modelling results only for a specific reference height (hub height) and do not include detailed profiles of the vertical atmospheric structure. Although it is theoretically important to differentiate between surface and high-altitude winds, this study was unable to quantitatively analyze this distinction owing to dataset limitations. The WS dataset has a resolution of 225 m, and wind speeds above 11 m s⁻¹ were excluded from the analysis. The wind speed layer is illustrated in Figure 3e.

High wind speeds were observed in Central Asia, the Himalayas, the coastal and mountainous regions of Japan, and around Taiwan, whereas relatively low speeds were found in inland South Asia, the Indian subcontinent, and the Arabian Peninsula.

2.1.7. Aerosol Optical Depth (AOD)

Aerosol Optical Depth (AOD) is defined as the total amount of light absorption and scattering in an atmospheric column up to a wavelength of 550 nm (Sayer et al., 2014). AOD is one of the most frequently used indicators for measuring the amount of aerosol present in the atmosphere (Koçak & Ebrahimi, 2020). This parameter, which is directly linked to sky clarity, increases when influenced by factors such as clouds and aerosols, reducing transparency (Varela et al., 2008). Therefore, the observation site should ideally have a low AOD. The MODIS instruments on the Aqua and Terra satellites provided datasets for the AOD products. The AOD datasets MOD04 L2, MOD04 3 K, and MYD04 3 K have spatial resolutions of 10 × 10 km and 3 × 3 km,

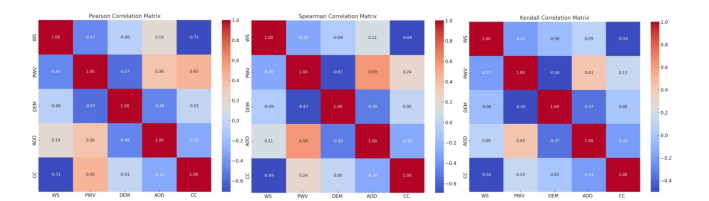


Figure 4. The correlation coefficients are calculated for the average annual changes of all GIS layers. The heatmap visually represents the strength and direction of correlations between the variables. The color coding scheme is as follows: Red indicates a positive correlation between 0.00 and 1.00 (highest), while blue indicates a negative correlation between 0.00 and -1.00 (lowest).

respectively. MODIS generates data as HDF4 files. The data were merged according to WGS84 DATUM standards and converted to GEOTIFF format using the GDAL library (Warp and Translate; Aksaker et al., 2020). High AOD values were concentrated in East Asia, especially in and around China. This can be linked to the high industrial activity and air pollution in this region. Low AOD was observed in the northern parts of Asia and in areas close to desert regions.

2.2. Correlations between GIS layers

The relationship between the parameters used in the selection of the astronomical location was analyzed using the annual average values of the countries' GIS layer. The relationships between the astronomical site selection parameters used in this study were analyzed using Pearson, Spearman, and Kendall (N= 48) correlations. The results of the analysis are shown in Figure 4 as matrices. The value +1 of the values calculated as a result of the correlation of the individual parameters (GIS levels) with each other indicates a strong positive relationship between the variables, while the value -1 indicates a strong negative relationship. Values close to zero indicate no significant relationship between the two variables. The existence of a relationship between the parameters with an absolute value of the correlation coefficient greater than 0.5 was assumed. From this perspective, we found three significant correlations in the analysis results (according to Spearman).

2.3. GIS-based multi-criteria decision analysis (MCDA)

The criteria used in this study were adjusted based on the criteria weights derived from the author's previous work using the BWM and FAHP-MCDA methods and expert opinions (for details, see Yılmaz, 2023b). In this study, the updated criteria weights were determined by averaging the weights calculated using both methods. The weights for the different telescope types were determined by proportionally distributing the criteria weights calculated using the BWM and FAHP-MCDA methods in accordance with the previous weights. The resulting criteria weights are presented in Table 3. Astronomical site selection studies aim to determine the most suitable sites for observational and research purposes. In determining the sites, variables such as atmospheric, anthropogenic, and geographic conditions were considered for each candidate site. The selection of a suitable site is possible by jointly analyzing the layers specific to potential astronomical sites. In this context, MCDA and GIS methods have been used together to analyze layers in many studies (Yılmaz, 2023a); (Yılmaz, 2023b), (Koc-San et al., 2013). While GIS organizes spatial data to solve complex problems in the process of astronomical site selection, the MCDA technique supports the

Table 3. Weighting of GIS layers in the MCDA analysis.

LAYERS	PWV	DEM	CC	AL	WS	AOD
IR WEIGHT	0.145	0.22	0.275	0.135	0.07	0.155
OPTICAL WEIGHT	-	0.26	0.32	0.16	0.08	0.18
RADIO WEIGHT	0.40	0.60	-	-	-	-

analysis and classification of these data (Sánchez-Lozano et al., 2013). The MCDA framework used in this study consisted of three levels: spatial organization, standardization, and aggregation. The GIS layers were standardized by transforming them to a common spatial resolution (1 km) using the 'Resample' tool in ArcGIS. Each layer was categorized into five levels, from 1 to 5. The criteria weights determined using the MCDA methods were used in the layer overlap phase (see Section 2 and Table 3 for details).

2.4. Scenarios

The design, performance, and efficiency of astronomical observatories are affected by their dependence on the wavelength. Different observatories must be designed for specific wavelength ranges, such as optical, infrared, and radio waves, and each requires different technological approaches and instruments. For example, the Next-Generation Very Large Array (ngVLA) is a synthesis radio telescope designed to operate at centimeter wavelengths, specifically in the 1.2 GHz to 116 GHz range (Selina et al., 2018).

The operational efficiency of telescopes (optical, infrared, radio, etc.) is significantly affected by environmental factors. Understanding these factors is important for optimizing observations and ensuring the quality of the collected data. Each type of telescope faces unique challenges depending on its wavelength range and atmospheric conditions under which it operates. When determining a potential location for an astronomical observatory for a telescope, numerous factors are considered that affect the quality of the observations. These include various anthropogenic, geographic, and atmospheric conditions, such as cloud cover, atmospheric water vapor, wind speed, altitude, light pollution, and optical aerosol density (Aksaker et al., 2020); (Sabil et al., 2010). Infrared telescopes face challenges related to atmospheric water vapor and thermal emissions (Swinyard & Nakagawa, 2009); (Liu et al., 2020) and are influenced by many anthropogenic, geographic, and atmospheric conditions. Radio telescopes are less affected by atmospheric conditions than optical and infrared telescopes but still face challenges such as radio frequency interference (RFI) and atmospheric conditions such as humidity and precipitation. As RFI detection requires many ground-based measurements and measurement points, it could not be used in this study. Each telescope type uses specific strategies and technologies to address these challenges and ensure optimal performance in its respective observation areas.

Therefore, it is important to use atmospheric layers created using GIS analyses when determining optimal areas. Different scenarios were created for the selection of astronomical areas depending on the telescope type. For optical telescopes (CC, WS, DEM, AOD, and AL), infrared telescopes (CC, DEM, PWV, AOD, WS, and AL), and radio telescopes (PWV and DEM), the layers were combined by weighted overlay by multiplying them with weights determined by MCDA methods based on expert opinion

(see Table 3). It is important to remember that the areas suggested for remote access methods need to be validated through field trials

For potential astronomical sites with optical telescopes, cloud cover and altitude are more important than other layers (Liu et al., 2020). Cloud cover is one of the most important layers in astronomical site selection (except in areas where radio and sub-mm telescopes are used) (Yılmaz, 2023a,b). For potential astronomical sites with infrared telescopes, almost all available layers should be used, as light propagation is always affected by atmospheric instability (Aksaker et al., 2024). Finally, potential astronomical sites with radio telescopes are less affected by atmospheric phenomena than sites with infrared and optical telescopes. In radio astronomy, all the water vapor in the atmosphere of the potential site can attenuate some radio frequencies, and low humidity and water vapor at high altitudes can enhance radio observations (Tremblin et al., 2012). Therefore, the selection of astronomical sites was diversified based on different scenarios.

3. Results and discussion

Calibrating satellite data is crucial for ensuring the precision and reliability of remote sensing applications. However, there is an ongoing debate surrounding the methods employed to identify extreme meteorological values (Easterling et al., 2016).

Using MCDA and GIS infrastructures, suitable astronomical sites in Asia were analyzed based on pixel values by weighting and overlapping different GIS layers, as proposed in Figure 5 (at a high spatial resolution: 1 km). In addition, the locations of observatories on the continent were analyzed using the created GIS layers. The study consisted of three main phases (Figure 2). In the first phase, we present the details of the satellite and model data used. In the second phase, the linking of the GIS layers with each other and the preprocessing of the data are explained. In the final phase, scenarios were created that suggest suitable areas for infrared, optical, and radio telescopes, which were determined using MCDA and GIS methods.

3.1. GIS layers

The annual average values of the astronomical GIS layer values used in the study for the parts within the boundaries of each country are given in Table 4. It can be observed that the atmospheric conditions for astronomical studies improve as we approach the Tibetan Plateau region.

A clear sky is important for astronomical observations and is expressed as the reciprocal of the cloud cover rate. It is important that the value of cloudiness is low. According to calculations, approximately 63 % of the year is cloud-free in the Asian continent. In regions where astronomical observation stations are located, this value decreased to 48

• The average PWV for Asia was 18.8 mm. This value is 15.1 mm on average for the astronomical observation stations, and it can be seen that the PWV value is below the continental average in approximately 81% of the stations.

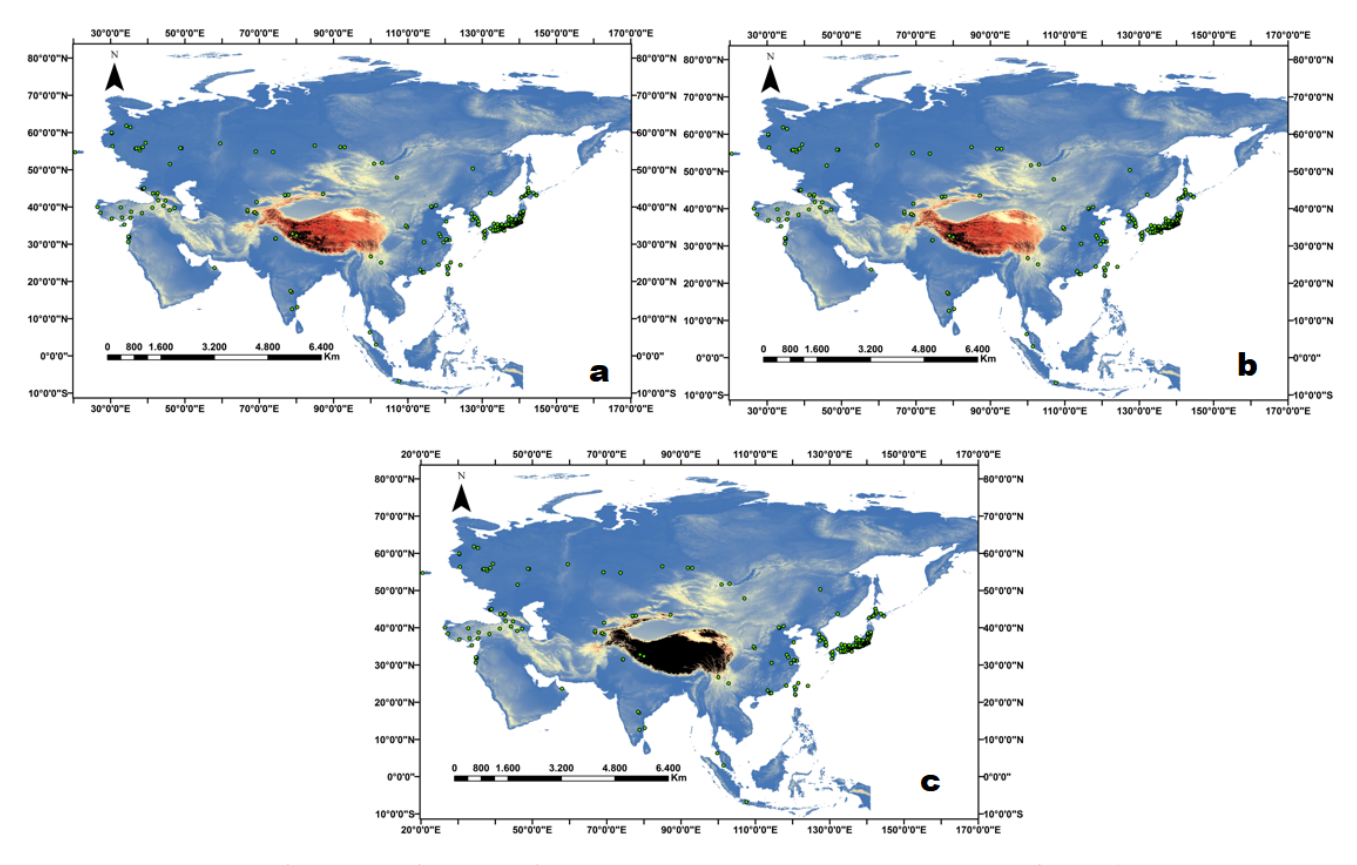


Figure 5. Shows the results of the scenarios for optical, infrared and radio telescopes that were created as a result of the GIS/MCDA analysis. The color scale was designed so that the quality of the locations ranged from poor (shades of blue, 1 point) to good (shades of orange, 4 points) to best (black color, 5 points). The observatories listed in Table 1 are marked with green dots on the maps. The most suitable areas for astronomical studies are highlighted in black color, and these regions are suggested as the best astronomical sites.

Table 4. Countries in Asia and average values of parameters used in the selection of astronomical sites.

Country	WS	PWV	DEM	AOD	CC	AL		Country	WS	PWV	DEM	AOD	CC	AL
	$(m s^{-1})$	(mm)	(m)		(%)	$(mag arcsec^{-2})$		$(m s^{-1})$	(mm)	(m)		(%)	$(magarcsec^{-2})$	
South Cyprus	2.56		15.06	378	0.27	0.22	19.7	Malaysia	1.29	42.71	279	0.30	0.70	19.34
KKTC	2.75		16.19	136	0.27	0.22	19.86	Indonesia	1.46	40.34	344	0.29	0.68	20.09
Yemen	3.62		20.14	943	0.30	0.15	20.6	Philippines	2.52	36.90	328	0.20	0.58	20.47
Oman	4.02		23.98	274	0.46	0.10	19.66	Taiwan	2.50	27.23	777	0.34	0.51	18.79
UAE	3.71		22.09	116	0.46	0.10	18.88	Myanmar	1.92	22.12	595	0.25	0.45	20.75
Bahrain	3.68		22.35	15	0.55	0.22	17.41	Bangladesh	2.65	24.80	28	0.59	0.44	20.51
Qatar	4.14		23.49	27	0.62	0.13	18.41	Bhutan	1.72	8.83	2816	0.12	0.49	20.71
Kuwait	4.85		18.47	119	0.42	0.17	18.57	Nepal	2.20	10.40	2084	0.26	0.38	20.72
Saudi Arabia	4.03		17.41	641	0.36	0.14	19.58	India	2.62	21.79	587	0.36	0.37	20.34
Jordan	3.93		11.83	766	0.20	0.13	19.42	Pakistan	3.11	17.59	1040	0.43	0.22	20.36
Israel	3.10		15.08	265	0.32	0.16	18.76	Afghanistan	3.52	9.92	1809	0.29	0.22	20.33
West Bank	3.02		15.13	338	0.35	0.19	18.90	Turkmenistan	4.34	16.81	201	0.27	0.31	19.84
Lebanon	2.85		11.31	997	0.22	0.23	19.25	Tajikistan	3.54	6.14	2963	0.23	0.35	20.41
Iraq	4.05		16.91	301	0.32	0.19	19.40	Kyrgyzstan	3.23	5.41	2650	0.20	0.41	20.27
Syria	3.87		13.62	516	0.23	0.21	20.36	Uzbekistan	4.11	14.60	349	0.33	0.34	20.10
Turkey	2.92		10.99	1141	0.20	0.34	20.19	South Korea	2.89	15.64	265	0.36	0.51	19.57
Armenia	2.72		9.10	1858	0.21	0.44	20.37	North Korea	2.95	10.05	594	0.23	0.46	20.86
Azerbaijan	2.53		15.52	646	0.26	0.50	20.18	Japan	2.98	15.59	387	0.26	0.61	19.69
Georgia	2.74		9.99	1236	0.15	0.53	20.16	China	3.62	10.88	1793	0.30	0.42	19.98
Iran	3.57		13.97	1256	0.34	0.22	20.02	Mongolia	4.04	6.19	1487	0.14	0.32	20.24
Vietnam	2.69		30.88	396	0.40	0.57	19.83	Kazakhstan	4.27	11.46	350	0.18	0.42	19.88
Cambodia	2.25		34.87	126	0.32	0.60	20.58	Russia	3.20	6.68	348	0.18	0.58	19.41
Thailand	2.47		30.45	286	0.37	0.53	20.20	Sri Lanka	3.23	35.79	176	0.25	0.55	20.54
Laos	2.37		24.01	669	0.40	0.49	20.81	Brunei	1.11	42.58	103	0.26	0.75	18.76

- The average wind speed (WS) calculated as $3.07~\text{m s}^{-1}$ for all locations in Asia. The average wind speed at the astronomical observation stations was $2.76~\text{m s}^{-1}$. The stations of the ISON-Terskol Observatory and the Starlab Observatory in Karachay-Cherkessia stand out as the astronomical stations with the highest values, with average wind speeds of almost $11~\text{m s}^{-1}$.
- While the average height in Asia is 745.8 m, this value averages 537.15 m at the astronomical observation stations. The Corona Borealis Observatory Ngari (4965 m) had the highest altitude value.
- While the average AOD value of the continent is 0.3, the average AOD value of the astronomical stations is 0.32.

Approximately 55% of the astronomical stations had AOD values below the continental average.

3.2. Correlations between GIS layers

The analysis of the relationships between the GIS layers is described in Section 2.2. The results of the three different correlation analyses are shown in Figure 4. Although the R^2 values in the three analyses showed small differences, similar trends were observed. The analysis results showed two strong correlations between the pairs of layers used in this study.

- There is a strong negative relationship between the percentage of cloud cover (CC) and wind speed (WS). This indicates that cloud cover decreases with increasing wind speed and vice versa.
- A negative linear relationship between DEM and PWV is expected (Aksaker et al., 2024). A higher DEM indicates a lower PWV. Otarola et al. (2019) and Aksaker et al. (2024) found a negative relationship between DEM and PWV in their studies.

4. Conclusion

Three different scenarios were created, and the criteria for each scenario were weighed differently (Table 3). All scenarios aimed

to achieve ideal weather conditions that could generate long observation periods. The most ideal locations in the scenarios had a value of 5 (see black areas in Figure 5). Higher site values therefore require sites with higher altitudes and lower cloud cover, AOD, PWV, WS, and AL values. On the continent, the Tibetan Plateau and its surroundings (with the exception of the area around 90 E-35N) in northern China have been identified as the most suitable areas for astronomical studies using radio telescopes. Suitable areas for infrared and optical telescopes are located in the southeast of the Tibetan Plateau (around 83E-31N) (see Fig. 5a and Fig. 5b). According to the analysis, an area of $369,096 \text{ km}^2$, which corresponds to approximately 0.83 % of the continent, is best suited for infrared observations. Of the total land area, 3.87 % (approximately 1,725,246 km²) is best suited for radio telescopes, while 0.8 % i.e. 355,842 km², is best suited for observations with optical telescopes (see Figure 5c). According to three different scenarios, the Corona Borealis Observatory (Ngari) and Himalaya Chandra Telescope (IAO Hanle) are located within the boundaries of the region with ideal conditions for astronomical observations (black dots in Figure 5). The Corona Borealis Observatory (Ngari) and the Himalaya Chandra Telescope (IAO Hanle) are in close proximity to each other. It can be said that the Corona Borealis Observatory (Ngari) has the most ideal location among the three scenarios, as it has the highest DEM value and the lowest CC value, and DEM and CC have high criterion weights (see Table 1).

■ APPENDICES

Table 5. Coordinates of astronomical stations in Asia and parameter values.

Astronomical Units	Longitude	Latitude	AL	WS	PWV	DEM	CC	AOD
Corona Borealis Observatory Ngari	80.026	32.326	0.43	4.98	1.90	4965	0.20	0.25
Himalayan Chandra Telescope IAO Hanle	135.136	33.923	0.45	4.70	46.13	4278	0.20	0.07
Lijiang Station Yunnan Observatories	30.295	59.942	0.45	4.14	14.28	3193	0.51	0.12
Eastern Anatolia Observatory DAG	136.308	35.208	0.62	7.32	5.48	2989	0.37	0.17
Takanezawa Tochigi	41.420	43.650	2.72	1.41	10.79	2820	0.62	0.22
ISON-Terskol Observatory	42.654	43.740	0.66	10.70	10.12	2810	0.49	0.22
Tokyo-Dodaira	76.972	43.057	0.74	2.89	15.63	2791	0.68	0.12
Assah Lulin Observatory	77.871 100.031	43.226 26.709	0.54 0.35	3.34 1.13	5.72 32.62	2662 2634	0.42 0.32	0.12 0.84
Lulin Observatory Tashkent	140.386	37.296	51.51	0.76	11.89	2581	0.54	0.84
Sumoto	133.544	34.672	5.13	2.00	15.53	2548	0.57	0.12
Madras	139.439	35.574	41.47	1.92	11.00	2522	0.55	0.30
Toyonaka	133.596	34.574	34.30	1.76	12.35	2401	0.55	0.19
Rostov	118.821	32.067	37.31	3.49	12.29	2121	0.45	0.28
Velikie Luki	139.909	36.563	12.90	2.36	12.10	2052	0.51	0.15
ISON-Kislovodsk Observatory	107.052	47.865	0.48	3.06	4.80	2048	0.44	0.10
Kislovodsk Mtn. Astronomical Stn. Pulkovo Obs.	118.313	24.433	0.49	3.95	12.24	2039	0.51	0.10
Saku	39.415	57.189	0.70	4.35	14.25	1975	0.59	0.13
Shishikui	138.179	34.818	0.72	1.53	18.58	1897	0.56	0.09
Omsk-Yogik Observatory	139.337	36.245	1.14	4.29	11.00	1892	0.37	0.23
Ka-Dar Observatory TAU Station Nizhny Arkhyz	37.883	55.248	0.42	3.96	16.21	1876	0.62	0.09
Engelhardt Observatory Zelenchukskaya Station	48.816	55.839	0.44	2.43	13.32	1857	0.44	0.09
Nanyo	113.323	23.144	5.95	2.25	19.37	1756	0.55	0.28
Shizuoka	140.006	36.184	6.49	10.31	14.69	1679	0.56	0.09
ISON-Hureltogoot Observatory	44.275	40.348	3.23	4.14	8.26	1628	0.48	0.11
Abastuman	42.820	41.754	0.62	1.43	10.56	1538	0.51	0.18
ISON-Byurakan Observatory	127.482	50.319	1.46	1.23	5.11	1538	0.38	0.29
Byurakan	44.292	40.335	0.70	1.23	10.70	1345	0.44	0.31
Kawane	140.021	36.867	0.40	2.21	37.70	1323	0.57	0.16
Nishi Kobe	140.159	38.045	7.12	2.87	11.28	1303	0.54	0.27
Kreiken Observatory	92.974	56.012	26.78	3.55	17.00	1255	0.61	0.25
Bosscha Observatory Lembang Shimotsuma	107.616	-6.826	6.12 3.79	1.08	26.44 8.78	1214 1192	0.57 0.59	0.22 0.23
Alma-Ata	134.891 76.957	35.128 43.188	13.21	1.31 1.48	6.01	1192	0.39	0.25
Yamamoto	30.515	56.322	1.01	1.53	11.38	1182	0.55	0.25
Minami-Oda Observatory	103.067	51.810	0.57	1.21	17.21	1156	0.66	0.45
Kiyosato	143.783	43.758	0.78	2.70	16.22	1103	0.59	0.14
Tokyo (before 1938)	44.789	41.717	100.66	2.16	8.92	1103	0.58	0.15
Uto Observatory	135.485	34.807	0.52	1.58	11.15	1094	0.61	0.37
KARAMAN	137.056	35.413	0.63	3.32	10.96	1086	0.59	0.19
Moscow	138.300	35.863	410.68	2.47	12.25	1086	0.54	0.25
Inönü University Observatory	136.133	34.769	5.57	1.58	38.84	1027	0.32	0.23
Bohyunsan Optical Astronomy Observatory	128.977	36.165	0.53	6.63	15.48	969	0.49	0.23
Yamagata	38.584	44.792	1.10	3.53	12.24	965	0.56	0.16
Ray Observatory	109.551	34.946	0.43	3.03	11.36	898	0.52	0.18
Gumma Astronomical Observatory	33.726	35.259	0.49	2.74	14.93	889	0.54	0.23
Vedrus Observatory Azovskaya	139.872	36.556	0.66	3.22	19.27	840	0.70	0.38
Miwa	134.720	35.095	0.43	2.44	23.94	834	0.58	0.53
Beijing Astronomical Obs BAO	117.575	40.394	0.74	1.31	11.52	825	0.40	0.22
Dushanbe	47.234	39.717	41.33	0.75	11.14	817	0.39	0.43
Akashina	137.949	36.329	0.70	1.57	11.31	812	0.53	0.26
JiangNanTianChi Observatory Mt. Getianling	140.250	35.919	3.01	2.52	8.48	807	0.42	0.29
Iwaki	132.166	43.698	0.49	4.43	25.25	744	0.39	0.21
Gissar Furukawa	128.887	35.253	3.29	0.92	17.25	725	0.39	0.34
Tokushima	135.177 120.890	35.268 23.487	0.69 1.11	1.33 2.31	15.30 11.50	709 705	0.63 0.63	0.23 0.25
Chichibu	139.150	25.487 35.989	0.91	1.43	12.41	677	0.63	0.23
Martin S. Kraar Observatory Rehovot	66.896	38.673	75.60	2.39	14.46	669	0.54	0.24
Kitab	42.662	43.742	8.69	2.39	12.39	654	0.57	0.23
Japal-Rangapur	140.599	36.960	0.68	2.56	11.78	641	0.62	0.23
Chirorin	137.896	36.762	0.84	2.16	13.40	635	0.59	0.20
Kuma Kogen	39.031	45.020	0.43	2.92	14.57	618	0.57	0.22
UZAYBIMER	30.333	36.825	58.15	2.51	6.02	601	0.38	0.23
Toyota	142.550	43.841	1.29	3.38	9.87	572	0.32	0.18
Adati	140.825	37.666	0.41	1.57	15.52	568	0.58	0.24
Oishi	99.781	6.307	0.56	2.11	11.90	568	0.69	0.16
Oisiii								
Hyderabad	69.122	54.878	44.48	1.97	17.19	534	0.40	0.45

Table 5. Coordinates of astronomical stations in Asia and parameter values (cont.)

		a una paramet	er values (cont.) $(nWcm^{-2}sr^{-1})$	(m s ⁻¹)	(mm)	(m)	(%)	
Ege University Observatory	74.444	31.514	3.04	6.86	15.69	485	0.29	0.27
Sayan Solar Observatory Irkutsk	69.218	38.261	0.50	3.04	13.53	485	0.57	0.27
Tataka Mt. Yu-Shan National Park	134.893	34.350	0.38	2.07	12.38	485	0.53	0.24
Petrozavodsk	116.328	40.101	24.88	3.16	21.42	484	0.65	0.71
Fushan Observatory Mt Shaohua	137.180	36.261	5.17	2.35	16.34	473	0.52	0.68
Sukagawa	139.853	36.507	4.97	2.60	16.70	466	0.55	0.38
Гаjimi	41.442	43.653	3.18	2.74	16.16	417	0.66	0.29
Wise Observatory Mitzpeh Ramon	35.350	37.060	0.49	2.03	19.05	392	0.73	0.34
Badalozhnyj Observatory	91.843	56.084	0.56	2.49	7.87	387	0.62	0.19
Bisei Spaceguard Center-BATTeRS	133.544	34.672	0.51	3.57	15.76	384	0.52	0.29
JCPM Oi Station	140.863	38.275	0.87	2.70	12.07	384	0.55	0.24
Murou	114.358	30.521	1.00	2.60	16.09	353	0.63	0.25
Mt. Guizi Observatory	135.990	35.050	38.36	2.01	11.24	350	0.56	0.29
Purple Mountain Observatory Nanking	113.964	22.377	9.87	3.86	12.79	325	0.39	0.24
MASTER-II Observatory Tunka	127.483	50.319	0.47	2.16	18.09	320	0.50	0.29
Kurohone	141.068	38.802	0.79	4.17	17.03	311	0.63	0.26
Ojima	135.340	34.133	2.36	1.01	9.17	306	0.59	0.32
Chinese Culture University Taipei	121.540	25.135	13.68	2.64	35.93	305	0.61	0.41
Kourovskaya	136.178	34.947	1.20	2.86	8.54	299	0.33	0.21
Gimhae Astronomical Observatory Uhbang-dong	138.995	35.125	6.70	5.82	11.31	298	0.52	0.45
Nyukasa	142.483	44.374	0.51	2.24	13.45	278	0.51	0.35
Gekko	133.828	33.527	1.17	2.88	16.96	273	0.58	0.27
CPM Sapporo Station	140.129	36.092	1.04	2.25	23.23	265	0.63	0.26
Hatamae	137.628	34.703	0.70	3.12	21.07	257	0.59	0.28
Bareket Observatory Macabim	35.032	31.888	30.52	2.53	16.13	256	0.20	0.35
Sobaeksan Optical Astronomy Observatory	137.521	34.984	0.53	1.56	12.98	247	0.40	0.31
Pulkovo	34.282	61.772	37.00	2.41	19.20	246	0.66	0.25
Don Astronomical Observatory Rostov-on-Don	41.233	39.783	0.42	1.54	17.28	229	0.52	0.23
Yatsugatake South Base Observatory	34.763	30.596	0.72	3.22	12.13	229	0.41	0.40
Kangwon Science High School Observatory Ksho	139.329	36.297	5.02	2.17	9.80	228	0.29	0.37
Vagatoro	135.925 41.233	33.610 39.783	2.09 20.00	2.00 1.55	11.98 23.35	220 213	0.69 0.28	0.27 0.69
Eden Astronomical Observatory Lahore Pujieda	41.428	43.656	0.56	1.33	18.28	209	0.28	0.09
Fokyo-Kiso	137.354	35.041	0.43	1.88	16.15	209	0.55	0.23
UZAYMER	139.039	35.690	18.14	2.88	18.88	208	0.60	0.15
Konan	141.087	38.540	3.36	2.67	17.01	206	0.64	0.38
Kawachi	140.523	35.899	10.04	2.14	36.94	204	0.49	0.25
ISON-Blagoveschensk Observatory	137.035	34.815	25.55	3.07	10.49	203	0.46	0.18
Purple Mountain Observatory XuYi Station	30.327	59.772	0.50	1.72	12.20	193	0.58	0.33
Yamada	78.826	12.576	3.17	2.57	12.23	193	0.56	0.31
Saratov	138.526	36.141	58.85	4.61	23.29	191	0.53	0.34
Melezhy Astrophoto Observatory	42.661	43.742	1.19	1.78	11.47	188	0.57	0.15
Dynic Astronomical Observatory	68.781	38.561	3.08	1.76	18.23	180	0.62	0.37
1st Moscow Gymnasium Observatory Lipki	36.955	55.771	17.88	2.63	10.96	178	0.62	0.26
Ka-Dar Observatory Barybino	119.600	30.469	11.27	4.02	16.58	177	0.54	0.23
Sanglok	134.122	35.339	0.55	2.91	14.62	176	0.56	0.31
ISON-Ussuriysk Observatory	42.500	43.275	0.60	3.21	15.35	175	0.55	0.22
Tokyo-Mitaka	134.241	34.090	18.75	9.21	16.03	167	0.55	0.34
Nachi-Katsuura Observatory	133.765	33.756	0.70	1.94	10.71	162	0.54	0.64
Special Astrophysical Obs SAO	138.421	35.020	0.45	2.98	11.23	158	0.56	0.30
Po Leung Kuk Observatory Tuen Mun	116.449	39.904	45.64	4.03	11.17	157	0.62	0.49
Гosa	139.542	35.672	2.82	3.06	18.01	154	0.61	0.25
ga-Ueno	78.454	17.432	13.03	2.02	10.61	152	0.56	0.40
Kitami	66.882	39.134	0.56	3.43	14.52	150	0.51	0.22
Hadano	138.973	36.596	16.36	1.93	14.52	149	0.58	0.30
Karasuyama	33.090	37.140	1.76	2.45	19.21	147	0.69	0.23
MASTER-II Observatory Blagoveshchensk	34.812	31.908	19.76	2.02	12.71	146	0.57	0.24
Krasnoyarsk	38.857	44.894	118.48	2.22	16.97	145	0.48	0.32
Nanshan Station Xinjiang Observatory	139.108	36.125	0.60	2.22	13.74	144	0.62	0.14
tarlab Observatory Karachay-Cherkessia	128.458	36.935	0.42	2.72	4.26	143	0.40	0.25
engamine	140.755	38.255	0.52	5.47	13.39	142	0.48	0.23
Miyasaka Observatory	138.468	36.496	1.04	1.84	17.61	141	0.60	0.73
Vanchuan Observatory Guangzhou	138.224	36.669	40.63	1.38	42.28	141	0.53	0.39
Asahikawa	142.421	43.743	11.57	2.21	10.62	139	0.62	0.35
CPM Kagoshima Station	140.338	38.185	7.04	2.75	11.01	139	0.62	0.26
Jtsunomiya-Imaizumi	120.320	36.070	26.76	1.27	15.03	137	0.11	0.30
Kwasan Observatory Kyoto	144.590	43.078	7.88	3.08	18.90	133	0.59	0.18
Horizon Observatory Petropavlovsk	139.247	36.228	66.96	3.86	24.35	131	0.53	0.23
Sendai Municipal Observatory	46.007	51.538	35.00	2.26	14.70	122	0.63	0.36
Jenohara	133.430	33.493	0.61	2.42	26.64	122	0.50	0.32
Ordubad	139.421	36.112	0.39	2.38	35.17	120	0.63	0.17
Oizumi	138.812	35.805	9.42	2.47	18.74	118	0.37	0.21

Table 5. Coordinates of astronomical stations in Asia and parameter values (cont.)

Table 5. Coordinates of astronomica	l stations in Asi	a and paramete		. 1				
			$(nWcm^{-2}sr^{-1})$	(m s ⁻¹)	(mm)	(m)	(%)	
ULTRA Observatory Suzhou	137.247	36.625	63.79	2.28	17.04	117	0.49	0.34
Tokai	69.294	41.325	0.90	2.45	15.02	116	0.54	0.36
Kahoku	136.914	34.987	1.15	2.22	11.12	113	0.55	0.40
Uzurano	120.627	31.303	2.05	2.94	16.30	111	0.66	0.17
Tokyo-Norikura	139.745	35.654	0.48	2.03	15.71	103	0.59	0.26
Purple Mountain Hainan Island station	35.343	61.404	2.77	3.21	17.69	101	0.52	0.19
Lvye Observatory Suzhou Engelhardt Observatory Kasan	120.873 27.270	23.469 38.400	6.17 9.09	4.36 2.75	16.40 11.38	99 98	0.55 0.56	0.43 0.24
Miyaki-Argenteus	138.937	35.171	1.86	3.90	17.94	98	0.57	0.24
Hong Kong Space Museum Tsimshatsui	139.314	35.370	3.23	1.11	10.98	96	0.57	0.31
Shinshiro	121.184	31.096	0.68	3.35	14.22	96	0.64	0.29
Kani	127.975	37.373	11.02	1.84	13.13	91	0.57	0.23
Petrozavodsk Univ. Obs. Sheltozero Stn.	117.575	40.394	0.55	3.32	13.60	91	0.59	0.73
Ishigakijima Astronomical Observatory	38.440	38.320	0.83	3.12	17.01	86	0.65	0.47
Kushiro	139.264	36.482	0.46	4.07	10.37	86	0.31	0.55
Tbilisi	137.088	35.343	82.59	1.61	14.77	83	0.58	0.46
KSA SEM Observatory Danggam-dong	32.780	39.840	24.36	3.06	20.06	81	0.57	0.81
BSH Byulsem Observatory Busan	129.082	35.263	18.94	2.26	17.71	75	0.57	0.42
Tomsk	137.625	35.797	64.39	1.93	23.14	75	0.58	0.53
Kasan	140.143	36.655	182.76	2.72	11.83	74	0.56	0.26
Sakamoto	140.655	42.645	3.97	2.41	14.83	72	0.58	0.24
Peking Transit of Venus site	140.946	38.566	82.30	2.60	21.99	69	0.57	0.17
Toma	139.194	36.006	1.02	2.74	13.73	68	0.55	0.47
KNUE Astronomical Observatory	139.521	35.767	3.24	2.15	14.58	67	0.57	0.41
Majdanak	80.246	13.069	0.43	4.05	17.32	64	0.58	0.16
Utsunomiya	137.257	35.135	14.00	1.65	18.89	64	0.60	0.34
Bibai	141.823	43.255	1.18	3.71	11.67	60	0.62	0.33
Green Island Observatory Gecitkale	34.815	32.070	5.04	2.11	11.70	58	0.21	0.28
Kumamoto	132.944	33.674	3.61	2.66	14.12	57	0.55	0.34
Tokyo-Asahikawa	42.501	43.275	7.47	3.34	17.16	57	0.64	0.38
JCPM Kimachi Station	142.321	45.112	32.78	1.86	16.04	54	0.57	0.42
Kiyose and Mizuho	138.448	35.899	26.95	2.01	16.64	52	0.61	0.31
Givatayim Observatory	68.682	38.490	75.11	1.99	16.51	50	0.19	0.58
Wakayama	35.550	38.710	20.14	4.82	11.98	50	0.50	0.33
Moriyama	130.449	33.290	19.21	2.36	16.67	48	0.55	0.20
Kamihoriguchi	20.495	54.713	10.90	2.24	14.58	47	0.56	0.39
Ootake	26.480	40.010	10.19	1.12	10.09	46	0.58	0.57
Nayoro Observatory Hokkaido University	87.175	43.474	1.33	2.69	11.66	43	0.55	0.11
Oosato	73.725	54.748	2.36	1.32	9.73	42	0.67	0.70
Al-Fulaij Observatory Oman	57.976	23.630	3.04	2.51	24.87	40	0.11	0.41
Ayabe	135.267	35.308	2.07	3.18	18.84	39	0.61	0.32
Honjo	114.323	22.408	2.91	2.47	9.56	39	0.54	0.44
Kagiya	41.426	43.650	14.97	2.70	12.49	35	0.60	0.47
Observatori Negara Langkawi	135.065	34.741	1.20	2.04	9.62	35	0.37	0.42
Fukuchiyama and Kannabe	138.188	34.902	1.20	2.62	13.30	34	0.61	0.34
Kenting Observatory Hengchun	120.698	22.050	6.95	5.43	8.35	34	0.37	0.35
Sapporo Science Center	135.868 140.862	35.068	59.60 14.24	2.46 3.62	17.52 13.97	34 33	0.60 0.56	0.44 0.31
Sheshan formerly Zo-Se Ochiai	138.175	38.259 35.900	0.44	1.14	16.23	31	0.56	0.31
Tokyo-Okayama	142.358	43.841	0.74	3.01	10.25	31	0.30	0.46
Geisei	109.824	34.508	0.74	2.05	15.04	30	0.24	0.46
Kuban State University Astrophysical Observatory	129.025	35.166	71.57	2.68	16.72	28	0.52	0.31
Sendai Astronomical Observatory	141.476	43.034	2.53	1.92	15.54	25	0.52	0.24
Cuteip Remote Observatory Changhua	120.557	24.093	32.41	2.47	25.50	23	0.33	0.78
JCPM Sakura Station	137.356	35.169	5.32	3.19	17.48	23	0.49	0.78
Mt. Kajigamori Otoyo	37.571	55.756	0.35	1.55	33.45	23	0.63	0.43
Osaki	132.221	34.221	13.81	1.74	10.70	23	0.52	0.14
Saji Observatory	118.464	32.734	0.50	1.49	3.91	23	0.52	0.40
Okutama	139.417	36.251	0.62	3.45	14.31	22	0.39	0.32
Krasnodar	59.547	57.037	11.25	3.56	10.78	21	0.55	0.17
Sendai Observatory Ayashi Station	100.921	51.620	7.53	0.66	17.45	21	0.56	0.31
Shimada	140.778	38.265	1.29	2.59	12.61	21	0.42	0.45
Nagano	136.014	34.570	9.13	2.06	16.76	20	0.51	0.39
Yatsuka	130.770	33.560	1.03	2.71	23.69	20	0.27	0.34
Ondokuz May University Observatory	139.083	35.814	0.81	3.14	12.84	19	0.66	0.42
Yatsugatake-Kobuchizawa	87.178	43.471	0.67	3.30	7.58	19	0.33	0.38
Kurashiki Observatory	130.753	32.676	17.02	1.65	11.62	18	0.55	0.49
Ageo	139.566	35.957	21.25	1.99	13.87	17	0.57	0.30
Kinmen Educational Remote Observatory Jincheng	120.784	21.950	17.32	4.73	11.77	16	0.54	0.61
Tien-Shan Astronomical Observatory	139.996	36.628	1.03	2.55	12.51	16	0.55	0.71
JCPM Hamatonbetsu Station	78.728	17.098	0.62	3.45	15.88	15	0.56	0.29
Peking Observatory Shaho Station	45.920	39.135	19.13	1.95	15.14	15	0.58	0.58
o coortaiory bilairo ballon	.5.,20	27.133	17.13	1.75	10.17	1.0	0.50	0.50

Table 5. Coordinates of astronomical stations in Asia and parameter values (cont.)

			` /					
			$(nWcm^{-2}sr^{-1})$	$(m s^{-1})$	(mm)	(m)	(%)	
Toyama	137.555	36.114	3.30	2.27	12.06	15	0.55	0.73
Kurihara	133.772	34.593	2.51	2.79	10.84	14	0.56	0.38
Machida	120.320	31.321	14.72	2.63	5.71	13	0.61	0.16
Hiratsuka	101.439	3.033	6.38	2.90	34.28	11	0.60	0.35
Tsingtao	84.947	56.468	69.94	7.35	16.77	10	0.29	0.72
Kaliningrad	140.310	38.442	62.23	2.75	12.94	9	0.51	0.19
Leningrad	135.793	34.995	199.48	3.13	23.07	9	0.57	0.05
Katori	49.121	55.790	1.98	3.36	13.80	8	0.53	0.34
Kochi	127.385	36.508	20.80	1.37	17.90	8	0.60	0.49
Kogota	133.527	33.552	1.26	3.58	8.67	6	0.49	0.45
Hin Hua Observatory Klang	78.964	32.780	58.12	1.46	15.24	5	0.71	0.54
Xingming Observatory Mt. Nanshan	134.871	34.951	0.65	2.18	21.25	5	0.60	0.34
Hidaka Observatory	140.720	38.309	1.01	2.56	2.02	4	0.65	0.33
Vainu Bappu Observatory Kavalur	135.958	34.409	0.51	3.53	14.98	3	0.61	0.54
Akou	134.393	34.749	18.59	2.69	15.72	2	0.74	0.44
Hamamatsu-Yuto	139.213	35.388	4.67	2.90	15.05	2	0.69	0.49
Kenting Observatory Checheng	138.079	35.141	2.13	5.53	30.13	2	0.63	0.49
Lulin Widefield Telescope Mt. Lulin	120.874	23.469	0.35	2.13	9.42	2	0.20	0.29
Yanagida Astronomical Observatory	135.172	34.214	0.44	2.04	12.80	2	0.49	0.33
JCPM Tone Station	141.367	42.913	2.48	3.58	11.32	1	0.61	0.29
Mishima	38.693	56.049	1.70	3.54	9.59	1	0.60	0.18
Southern Utsunomiya	134.319	33.551	11.23	4.22	13.79	1	0.31	0.40
Ishiki	124.139	24.373	5.27	2.57	8.32	-18	0.74	0.42

■ REFERENCES

- Ackerman, S. A., Holz, R. E., Frey, R., et al. 2008, JAtOT, 25, 1073, doi: 10.1175/2007JTECHA1053.1
- Aksaker, N., Bayazit, M., Kurt, Z., et al. 2024, ExA, 58, 4, doi: 10.1 007/s10686-024-09951-x
- Aksaker, N., Yerli, S. K., Erdoğan, M. A., et al. 2020, MNRAS, 493, 1204, doi: 10.1093/mnras/staa201
- Aksaker, N., Yerli, S. K., Erdoğan, M. A., et al. 2015, ExA, 39, 547, doi: 10.1007/s10686-015-9458-x
- Azhar, M. A. D. M., Hamid, N. S. A., Kamil, W. M. A. W. M., & Mohamad, N. S. 2022, Jurnal Teknologi (Sciences & Engineering), 84, 33, doi: 10.11113/jurnalteknologi.v84.19328
- Badger, J., Hahmann, A., Larsén, X. G., et al. 2015, The Global Wind Atlas: An EUDP project carried out by DTU Wind Energy
- Box, E. O., & Choi, J. 2003, Climate of Northeast Asia, ed. J. Kolbek, M. Šrůtek, & E. O. Box (Dordrecht: Springer Netherlands), 5–31, doi: 10.1007/978-94-017-0143-3_2
- Bustos, R., Rubio, M., Otárola, A., & Nagar, N. 2014, PASP, 126, 1126, doi: 10.1086/679330
- Chen, T., Li, Z., Kahn, R. A., et al. 2021, ACP, 21, 6199, doi: 10.5 194/acp-21-6199-2021
- Easterling, D. R., Kunkel, K. E., Wehner, M. F., & Sun, L. 2016, Weather and Climate Extremes, 11, 17, doi: https://doi.org/10.1016/j.wace.2016.01.001
- Erasmus, D. A., & Peterson, R. 1997, PASP, 109, 208, doi: 10.1086/ 133873
- Falchi, F., Cinzano, P., Duriscoe, D., et al. 2016, SciA, 2, e1600377, doi: 10.1126/sciadv.1600377
- Firth, P. G., Zheng, H., Windsor, J. S., et al. 2008, BMJ, 337, 2654, doi: 10.1136/bmj.a2654
- Gesch, D. B., Verdin, K. L., & Greenlee, S. K. 1999, Eos, Transactions American Geophysical Union, 80, 69, doi: 10.102 9/99EO00050
- Glickman, T. S. 2000, Glossary of Meteorology (2nd ed.; Boston, MA: American Meteorological Society)
- Gurbuz, G., & Jin, S. 2017, IJCli, 37, 5170, doi: 10.1002/joc.5153 Holz, R., Ackerman, S., Nagle, F., et al. 2008, JGRD, 113, 8, doi: 10.1029/2008JD009837
- Houze Jr, R. A. 2012, RvGeo, 50, 1001, doi: 10.1029/2011RG000365 Koc-San, D., San, B., Bakis, V., Helvaci, M., & Eker, Z. 2013, AdSpR, 52, 39, doi: 10.1016/j.asr.2013.03.001
- Koçak, T., & Ebrahimi, F. 2020, Ulusal Çevre Bilimleri Araştırma Dergisi, 3, 119
- Li, Z., Muller, J.-P., & Cross, P. 2003, JGRD, 108, 20, doi: 10.1029/ 2003JD003372
- Liao, L., Weiss, S., Mills, S., & Hauss, B. 2013, JGRD, 118, 12, doi: 10.1002/2013JD020475
- Liu, L., Yao, Y., Vernin, J., et al. 2012, in Ground-based and Airborne Telescopes IV, ed. L. M. Stepp, R. Gilmozzi, & H. J. Hall, Vol. 8444, International Society for Optics and Photonics (SPIE), 844464, doi: 10.1117/12.926157
- Liu, L.-Y., Yao, Y.-Q., Wang, Y.-P., et al. 2010, RAA, 10, 1061, doi: 10.1088/1674-4527/10/10/009
- Liu, L.-Y., Yao, Y.-Q., Yin, J., et al. 2020, RAA, 20, 084, doi: 10.108 8/1674/-4572/20/6/84
- Nag, S. 2015, RCC Perspectives, 3, 25, doi: 10.5282/rcc/7317
- Nan, R. 2006, Sci China Ser G, 49, 129, doi: 10.1007/s11433-006-0 129-9
- Otarola, A., De Breuck, C., Travouillon, T., et al. 2019, PASP, 131, 045001, doi: 10.1088/1538-3873/aafb78

- Platnick, S., King, M. D., Ackerman, S. A., et al. 2003, ITGRS, 41, 459, doi: 10.1109/TGRS.2002.808301
- Prange, C., & Kattenbach, R. 2019, Management practices in Asia: Case Studies on Market Entry, CSR, and Coaching (Springer Nature), doi: 10.1007/978-3-030-19662-2
- Radionov, V., Lamakin, M., & Herber, A. 2002, IzAOP, 38, 179 Ravi, S., & D'Odorico, P. 2005, GeoRL, 32, doi: 10.1029/2005GL02 3675
- Sabil, M., Benkhaldoun, Z., Lazrek, M., et al. 2010, A&A, 522, A69, doi: 10.1051/0004-6361/201014270
- Sánchez-Lozano, J. M., Teruel-Solano, J., Soto-Elvira, P. L., & García-Cascales, M. S. 2013, RSERv, 24, 544, doi: 10.1016/j.rser .2013.03.019
- Sarazin, M., Graham, E., & Kurlandczyk, H. 2006, Msngr, 125, 44
 Sayer, A., Munchak, L., Hsu, N., et al. 2014, JGRD, 119, 13, doi: 10
 .1002/2014JD022453
- Schueler, C. F., Clement, J. E., Ardanuy, P. E., et al. 2002, in Earth Observing Systems VI, ed. W. L. Barnes, Vol. 4483, International Society for Optics and Photonics (SPIE), 11 23, doi: 10.1117/12.453451
- Seidel, J. V., Otarola, A., & Théron, V. 2023, Atmos, 14, 1511, doi: 10.3390/atmos14101511
- Selina, R. J., Murphy, E. J., McKinnon, M., et al. 2018, in Ground-based and Airborne Telescopes VII, ed. H. K. Marshall & J. Spyromilio, Vol. 10700, International Society for Optics and Photonics (SPIE), 107001O, doi: 10.1117/12.2312089
- Sultan, M., Sturchio, N., Al Sefry, S., et al. 2008, Journal of Hydrology, 356, 70, doi: 10.1016/j.hydrol.2008.04.001
- Swinyard, B., & Nakagawa, T. 2009, ExA, 23, 193, doi: 10.1007/s1 0686-008-9090-0
- Tremblin, P., Schneider, N., Minier, V., Durand, G. A., & Urban, J. 2012, A&A, 548, A65, doi: 10.1051/0004-6361/201220420
- Varela, A., Bertolin, C., Muñoz-Tuñón, C., Ortolani, S., & Fuensalida, J. 2008, MNRAS, 391, 507, doi: 10.1111/j.1365 -2966.2008.13803.x
- Várnai, T., & Marshak, A. 2012, AMT, 5, 389, doi: 10.5194/amt-5 -389-201210.5194/amtd-4-6861-2011
- Walker, J. 1894, The Geographical Journal, 3, 339, doi: 10.2307/17 73701
- Ye, Q.-Z. 2011, PASP, 123, 113, doi: 10.1086/658201
- Yılmaz, A. 2023a, CoSka, 53, 28, doi: 10.31577/caosp.2023.53.1.28

 —. 2023b, SerAJ, 207, 39, doi: 10.2298/SAJ230530001Y